Ion energy analysis of a bipolar HiPIMS discharge using a retarding field energy analyser

F. Walk[1,2], R. Valizadeh[2] and J.W. Bradley[1]*

1 Department of Electrical Engineering and Electronics, University of Liverpool, Brownlow Hill, Liverpool, L69 3GJ, United Kingdom

2 STFC Daresbury, Warrington, Cheshire, WA4 4AD, United Kingdom

*Author for correspondence j.w.bradley@liv.ac.uk

Abstract

The time evolution of the positive ion energy distribution functions (IEDF's) at the substrate position in an asymmetric bipolar high-power impulse magnetron (HiPIMS) system was determined using a gridded energy analyser. This was done for a range of operating conditions, namely the positive voltage U_{rev} and "on-time" negative pulse duration τ_{neg}. The magnetron sputtering discharge was equipped with a Nb target. Based on the knowledge of the IEDF's, the bombarding ion flux density Γ_i and energy flux density Q_i to a grounded surface were calculated. Time-resolved IEDF measurements showed that ions with energies approaching the equivalent of the positive pulse voltage U_{rev} were generated as the reverse positive voltage phase developed.

On time-average, we observed that increasing the set U_{rev} value (from 0 to 100 V), resulted in a marginal decrease in the ion flux density Γ_i to the analyser. However, this is accompanied by a 5-fold increase in the ion energy flux density Q_i compared to the unipolar, U_{rev} = 0 V case. Reducing the negative HiPIMS pulse duration τ_{neg} (from 130 to 40 µs) at a constant discharge power leads to a modest increase in Γ_i, but a 4-fold increase in Q_i. The results reveal the benefit of the bipolar HiPIMS technique, in which it is possible to control and enhance the power density of ions bombarding a grounded (or fixed bias) substrate, for potentially better tailoring of thin film properties.

1. Introduction

In the sputter deposition of thin films, controlling the bombarding positive ion energy at the substrate is useful for tailoring the specific microstructures, crystallographic orientations and phases [1]. For electrically conducting samples, this is commonly achieved through substrate biasing, in which a negative potential (typically < 150 V) is applied to accelerate positive ions to significant energies upon bombardment of the growing film.

In conventional magnetron sputtering (DC or pulsed DC), the flux of ionic species at the substrate is dominated by inert gas ions (e.g. Ar^+), with only small fractions of ionized sputtered species arriving at the growing film [2].The flux of neutral sputtered atoms largely dictates the film deposition rate. Accelerating inert-gas ions delivers energy to the thin film growth process, promoting surface atom diffusion, enhancing densification and reducing the need for substantial substrate heating in many cases [3].

The introduction of high-power impulse magnetron sputtering (HiPIMS) [2], in which very high fractions of ionized metal ions are created in a dense plasma, has changed somewhat the ion-assisted growth process to one where it is the metal ions (with high bombarding energies) rather than metal neutrals (with relatively low bombarding energies) dominate the composition of depositing species.

This has the benefit that the energy of bombardment of the depositing species (i.e. metal ions) can be controlled and guided with a reduction in gas incorporation in the thin film [4] [5]. In many cases, this leads to improved thin film properties compared to earlier DC and pulsed methods. However, accelerating ions via substrate biasing is not achievable for electrically insulating films, dielectric substrates, highly complex geometries or when the substrate is grounded through deposition chamber design.

If external biasing of a sample is not possible, one method to generate high energy ions bombarding at a substrate is to elevate the potential of the plasma (in which ions

are created) above that of the (fixed) voltage substrate. This method has been investigated recently for HiPIMS plasmas, in a process named asymmetric bipolar HiPIMS in which a reverse (positive) voltage U_{rev} is applied to the cathode target, a short period after the primary negative sputtering pulse has terminated, so lifting the plasma potential V_p above that of the substrate [6] [7] [8]. Not only does this provide high energy metal ion bombardment of the growing film, but it can also increase the deposition rate. However, this technique is not guaranteed to produce accelerated ions to insulating thin film as the surface potential my float up to a potential close to, but just below that of the plasma. The conditions required to successfully achieve energetic bombardment, in this case, has been considered based on the effective capacitive coupling of the substrate to ground [9].

Extensive studies have been made to understand the basic plasma processes occurring during the reverse positive pulse period leading to high energy ions. These include measurements of the spatial-temporal evolution plasma potential due to the positive pulse. In some cases, depending on the system conditions, it is found that V_p is raised up uniformly everywhere in the plasma to a potential close to the positive voltage U_{rev} on the target [8] [10], while in other cases, a double-layer like structure is created in the bulk which travels from target to substrate [7] [11] [12]. In the former case, ion acceleration to the thin film occurs in the plasma sheath created between the plasma with a positive potential and the fixed bias substrate (e.g. ground potential). However, this may not provide energetic bombardment if the surface follows V_p. In the latter case, ion acceleration occurs within the double layer. With creation of such double layer accelerated ions, one can achieve energetic ion bombardment of insulating (electrical floating) substrates [13].

Recent studies of asymmetric bipolar HiPIMS have shown clearly that during the reverse positive bias pulse metallic and gas ionic species can be generated in the plasma at potentials up to U_{rev} which appear as high energy ions in tail of the ion energy distribution function (IEDF) when measured against ground potential [6] [14] [15]. Some such studies have shown the importance of the duration of the negative (on-time) pulse τ_{neg}. For instance, variation of τ_{neg} can be used to optimize the ion flux fraction arriving at the substrate. In particular, reducing τ_{neg} to 10 µs was shown

to eliminate the presence of low energy titanium ions in the measured IEDF [14]. Typically, these studies are carried out using energy-resolved mass spectrometry, with instruments such as the HIDEN EQP. Despite, the excellent energy and mass resolution obtainable with these instruments they are inherently perturbing to the plasma under investigation. Also, the large size of the instrument poses the problem of restricted access to the plasma via chamber ports, especially for complex vessel shapes. One other drawback is that the measured IEDF's are not absolutely calibrated so that the arriving flux density of the mass-selected ions is not known. However, there have been successful attempts to calibrate such instruments [16].

Here, we use a gridded retarding field energy analyser (RFEA) to determine the IEDF's for ions arriving at the substrate position in a bipolar HiPIMS plasma. The instrument is small, and although the measured ion currents and derived IEFD's are not mass resolved, we can determine the absolute flux density of arriving ions to within an acceptable accuracy and a sub-microsecond acquisition time. From the IEDF we can calculate the total bombarding ionic flux density and energy flux density with a time-resolution of 10 μs. Such analysers have been used to good effect over the years to diagnose plasmas, for example in, tokamak edge regions [17], capacitive and inductively-coupled RF systems [18], DC and pulsed DC magnetrons [19].

2. Experimental arrangement

The experimental setup consists of an unbalanced type 2 circular magnetron assembly fitted with a 7.6 cm diameter niobium target, housed in a stainless-steel cylindrical vacuum of internal diameter 27 cm and length of 30 cm. A schematic diagram of the magnetron assembly and magnetic field lines is shown in figure 1 a). The magnetic null position on the centerline is 3.5 cm from the magnetron target.

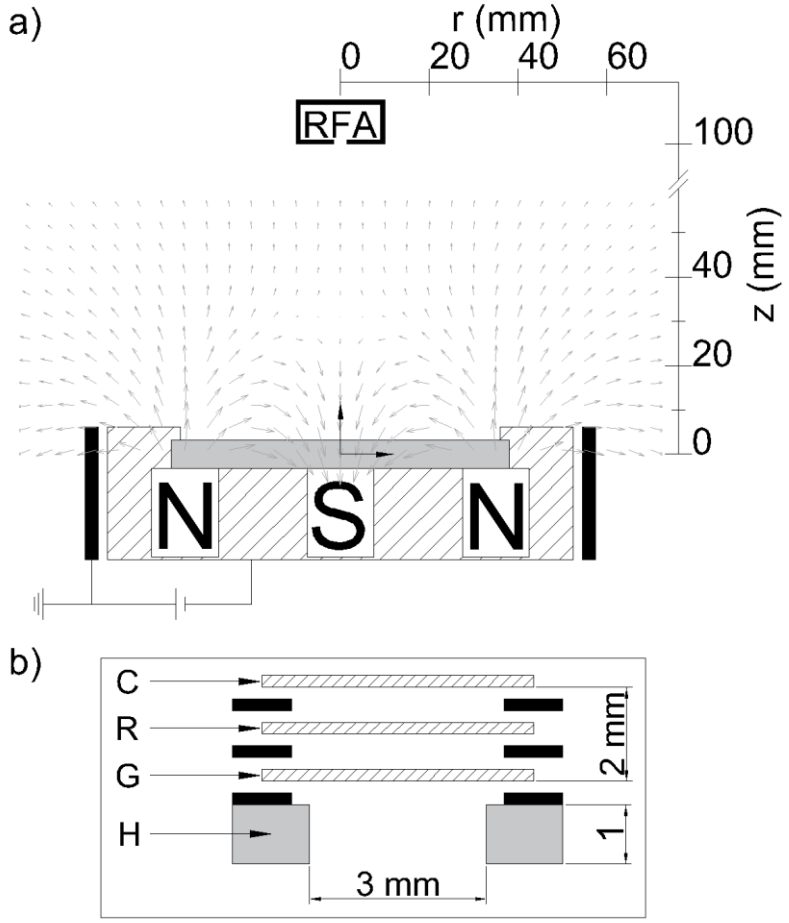

Figure 1 (a) A schematic diagram of the magnetron assembly, the magnetic field lines and position of the RFEA, (b) A diagram of RFEA construction, with ion collector (C), electron repelling grid (R), grounded outer mesh (G) and the housing (H) with a 3mm wide acceptance orifice.

The RFEA was placed perpendicular to the cathode target plane on the central axis away 10 cm from the target surface, corresponding to the typical substrate position. The vacuum system was pumped to a base pressure of 10^{-7} Torr by an Edwards EXT75DC turbo pump backed by 200 $Lmin^{-1}$ Pfeiffer DUO 10 MC rotary pump. The target was sputtered in argon gas with a purity of >99.998% at gas flow rates of 30, 40 and 50 sccm, to provide system pressures of 0.66, 1.33 and 2 Pa respectively, measured by a MKS 627A Baratron. The magnetron sputtering discharge was powered by a Starfire Industries Impulse 2-2 (bipolar HiPIMS unit),

which generated the required pulse voltage profiles. This unit was powered by a DC power from a 1.5 kW supply (Kurt J. Lesker PD500x3). The bipolar HiPIMS unit is capable of supplying a reverse positive voltage pulse U_{rev} from 0 to 200 V. The DC power supply controls the average power during the negative pulse. The average discharge power P_{avg} was kept constant at 200 W. The pulse frequency was fixed at f = 100 Hz.

A plot of the typical bipolar HiPIMS discharge voltage and current waveforms are shown in figure 2 with the important features highlighted, namely the negative pulse length τ_{neg}, the positive pulse length τ_{pos}, the delay time between the positive and negative pulses τ_d, the reverse positive voltage U_{rev}. In figure 2, we see that during the positive voltage pulse, the discharge current reverses peaking at about -5 A within the first 10 µs and then decaying slowly. This current is terminated once the positive voltage pulse ends. From figure 2 we can also see that the rise-time of the positive voltage pulse depends on U_{rev} itself, with the positive voltage attaining its maximum more quickly for U_{rev} = 100 V than for U_{rev} = 50 V.

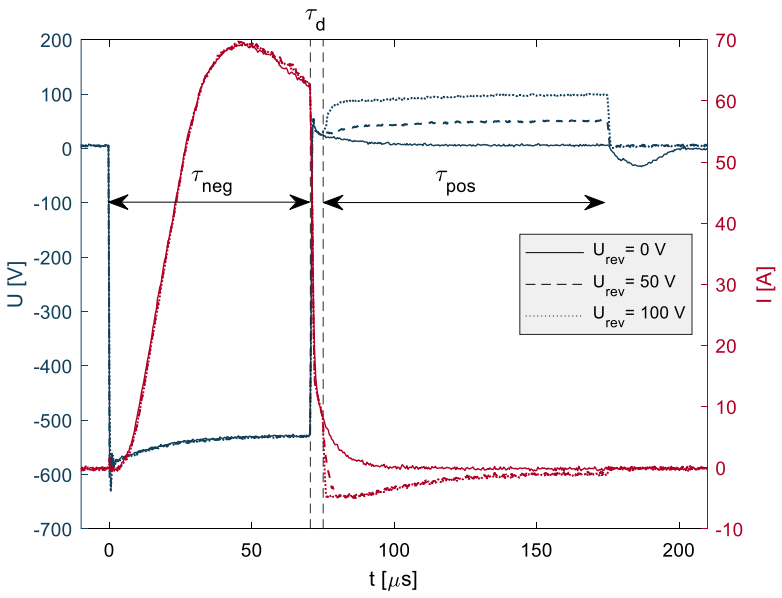

Figure 2. Discharge voltage and current waveforms for a bipolar HiPIMS with τ_{neg} = 70 µs and positive pulse of τ_{pos} = 100 µs with a varied reverse positive voltage U_{rev} between 0 and 100 V. The pressure was 0.66 Pa.

In this study, a number of these operating parameters are fixed, namely pressure P = 0.66 Pa, τ_d = 5 µs, τ_{pos} = 100 µs, while τ_{neg} was varied between 40 and 130 µs. U_{rev} was changed varied between 0 and 100 V. We could only use a maximum of 100 V due to the limitation of the sweeping voltage of the RFEA acquisition electronics. The discharge voltage and current measurements were made using a Tek P5100 (2.5 kV), high-voltage probe and a Pearson 3972 (0.1 V/A) current probe connected to a Tektronix DPO 3034 (300 MHz, 2.5 GS/s) oscilloscope.

The retarding field energy analyser (RFEA) was built in-house and consisted of a two G600 HSS Nickel TEM meshes and collector plate set-up, similar in design to that used by Ingram and Braithwaite [20] and more recently by Poolcharuansin [21], see figure 1b). The total length of the mesh-plate construction inside the RFEA was kept below 5 mm to minimize ion-neutral atom collisions within the analyser. The meshes were glued to thin metal-washers by conductive silver paint and insulated from the collector plate (C) using Kapton washers. The entrance orifice of the analyser had a diameter of 3 mm. These parts were push-fitted into an aluminum housing (H) with entrance of depth 1 mm. The two TEM meshes (G and R) had a total diameter of 3.05 mm with an exposed mesh area the same as the entrance office and a rectangular hole size of 37 µm x 37 µm offering a grid transparency of 78 %. The hole size of the mesh was chosen such that it was no more twice the typical Debye length, to prevent the plasma from entering the device and ensuring conductance of an ion beam to the collector plate. Independent Langmuir probe measurements in the plasma over the chosen magnetron operating conditions yielded calculated Debye lengths from 20 to 60 µm.

The outermost mesh (G) was electrically grounded to represent a grounded substrate. The second mesh (R) acts as an electron repelling grid, which was biased to a potential of U_{rep}= -300V to maximize the collector ion current. To measure the ion current I_c and discriminate between the arriving ion energies

a commercial Langmuir probe acquisition system (ESPION Advanced Langmuir Probe system) was used, connected to the ion collector (C) of the RFEA. The resulting time-resolved current-voltage curves yielded the ion velocity distribution function (IVDF) $f_i(v)$ by taking the first derivative of I_c in respect to the discriminating voltage V_d:

$$f_i(v) = -\frac{M_i}{\chi e^2 A}\frac{\mathrm{d}I_c}{\mathrm{d}V_d} \quad (1)$$

where M_i is the ion mass, χ the total transparency of the grids for ions, and e the electronic charge. The ion velocity v is related to the discriminating voltage V_d by:

$$v = \sqrt{\frac{2eV_d}{M_i}} \quad (2)$$

and is used to obtain the IVDF curve as discussed by Allen [22]. Other fundamental information can be extracted from the sampled ions by integrating the IVDF as follows:

The ion flux density

$$\Gamma_i = \int_0^\infty v f_i(v)\,\mathrm{d}v \quad (3)$$

and the ion energy flux density Q_i (equivalent to the power density, Wm^{-2})

$$Q_i = \int_0^\infty \frac{1}{2} M_i v^2 . v f_i(v)\,\mathrm{d}v. \quad (4)$$

The ion energy distribution function $f_i(\varepsilon)$ can be calculated from the ion velocity distribution function $f_i(v)$ using:

$$f_i(\varepsilon) = \frac{1}{\sqrt{2M_i\varepsilon}} f_i(v) \quad (5)$$

where $\varepsilon = eV_d$ is the kinetic energy of singly charged ions.

The obtain quantitative information on Γ_i and Q_i for different HiPIMS pulse parameters the RFEA must be calibrated. This was done by comparing the total RFEA ion current I_c (with V_d= -100 V) to that collected by a cylindrical Langmuir probe at nominally the same location in the plasma. At any plasma condition, even considering the mesh transparencies, it was found that the RFEA underestimated the ion current density compared to the ion saturation current density measured by the Langmuir probe. The loss could be due to ion-neutral collisions within the analyser, a lack of ion beam collimation within the RFEA, a reduced sampling of plasma ions due to a finite solid angle of collection or a misalignment between the two plates holding the TEM grids. From our measurements, we calculate an experimentally determined effective overall transparency $\chi \sim 0.11$ to be used in equation 1.

3. Results

3.1 The effect of U_{rev} on $f_i(E)$, Γ_i and Q_i at a grounded electrode

Using the RFEA the time-evolution of the ion energy distribution function, $f_i(E)$, ion flux density Γ_i and energy flux density Q_i have been determined for a variation of negative pulse durations τ_{neg} and reverse positive pulse voltages U_{rev}, while τ_{pos} was fixed at 100 µs.

Figure 3 shows the mass-integrated evolution of the IEDF's for U_{rev} = 50 and 100 V with τ_{neg} = 70 µs. During the HiPIMS "on-time" $f_i(E)$ is dominated by low energy ions mainly between 2 to 5 eV, presumably mostly argon gas ions, and a high energy tail with ions reaching 35 to 40 eV, we assume consisting of fast post-ionized sputtered niobium. Such IEDF's are seen in conventional HiPIMS plasmas [2]. At t = 80 µs (i.e. 5 µs into the positive voltage pulse) high energy ions appear in the distribution, with relative broad peaks. These shift to high energy at longer times into the positive pulse period. The highest ion energies obtainable increase as U_{rev} is increased from 50 to 100 V, as we may anticipate, however,

maximum obtainable energy is some 10 eV less than the energy equivalent of U_{rev}.

Inspection of the IEDF's shows that for U_{rev} = 50 V there is a gradual decrease in the peak intensity of high energy ions throughout the positive pulse of 100 µs duration. However, for U_{rev} = 100 V the peak intensities fall below the detection limit of the analyser after only 50 µs into the positive pulse.

The lower part of Figure 3 shows a projection (superposition) of all the time slices of the IEDF's recorded for the positive pulse period (t > 80 µs) only. For the smaller reverse voltage and the slower positive voltage rise time of U_{rev}, one can see copious amounts of low energy ions generated at the beginning of the voltage reverse. These low energy components are not produced in the U_{rev} =100 V case in which the fast rise time of U_{rev} to its maximum value is much faster. In both U_{rev} cases, the integrated counts in the IEDF's decrease by an order of magnitude within the first 50 µs of initiation of the positive pulse.

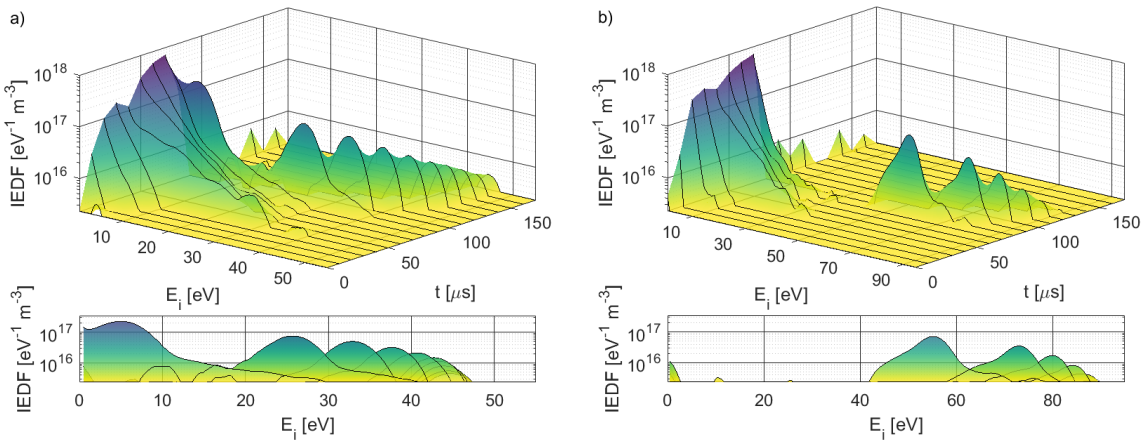

Figure 3. Plots of the temporal evolution of the IEDF's with τ_{neg} = 70 µs for the cases, a) U_{rev} = 50 V and b) U_{rev} = 100 V. The lower plots are a superposition of all the time slices recorded only during the positive pulse duration, t > 80 µs.

To explore the mechanism of high energy ion generation during the positive pulse period, the time-evolution of the plasma V_p and floating V_f potentials have been measured using a Langmuir probe at the position of the RFEA. The plasma

potential was determined to be voltage on the probe at which the first derivative of the probe current with respect to voltage, dI(V)/dV, was a maximum. These values are shown in figure 4 and are overlaid on a 2D colour map of the IEDF intensities, taken from the data shown in figure 3a. In figure 4 V_p and V_f are shown on the same y-axis as E_i, the RFEA measured ion energies.

During the negative HiPIMS pulse (t < 75 µs) the plasma potential V_p is close to ground potential and a strong peak in ions with energies up to 30 eV are seen. These correspond to post-ionized sputtered metals from the target. In the positive voltage pulse period (t > 80 µs) V_p and V_f both rise, with the former reaching a value just above 45 V. This trend fits perfectly well with the blue colour on the IEDF map representing the peak in the IEDF intensities. The direct correlation between V_p and peak ion energies indicates strongly that the high ion energies are a result of acceleration in the sheath that exists between the local plasma and the grounded entrance grid (G in figure 1) of the RFEA. This type of behavior is reported in Hippler et al. [8] and Viloan et al. [10]. As V_p increases during reverse positive HiPIMS pulse so does the sheath potential and its thickness. There is no direct evidence that a double layer-like structure exists in the plasma accelerating these ions. At the termination of the positive pulse, V_p falls dramatically to about 0.5 V, consistent with a normal afterglow.

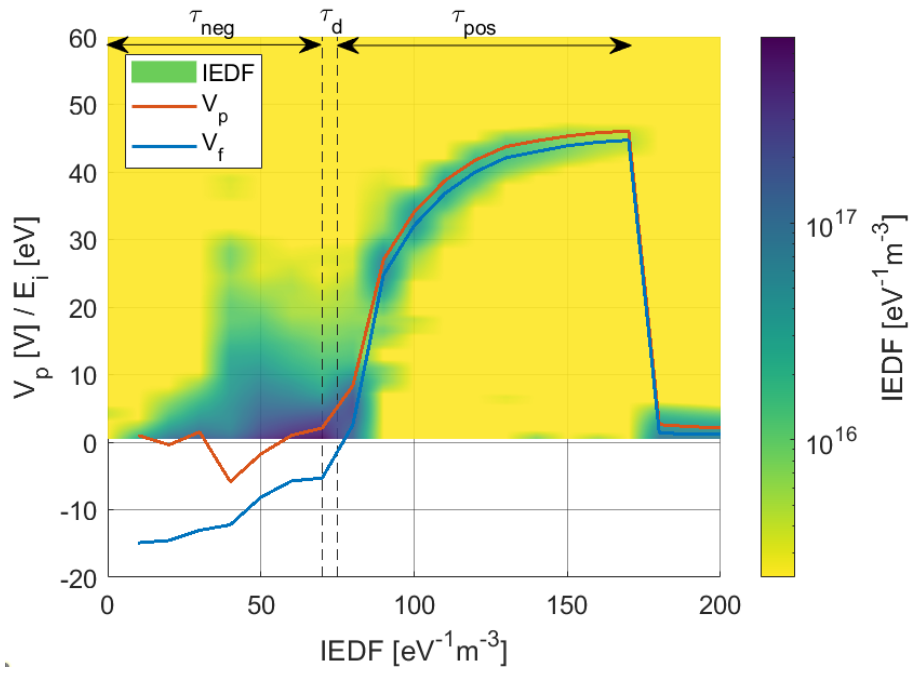

Figure 4. A plot of the plasma and floating potentials measured using a Langmuir probe at the RFEA position versus time during the HiPIMS negative and positive pulse periods, overlaid onto a colour map of the IEDF intensities. Here τ_{neg} = 70 µs and U_{rev} = 50 V.

During the deposition of thin films using the bipolar HiPIMS technique, the time-averaged bombarding ion energies will be important. The time-averaged IEDF's for the case τ_{neg} = 70 µs and U_{rev} = 0, 25, 50, 75 and 100 V are shown in Figure 5. These plots include contributions from both the negative and positive voltage phases of HiPIMS waveform. For the standard unipolar HiPIMS case (U_{rev} = 0) the low ion energy peak is the broadest because of the additional low energy ions present in the afterglow. Applying and increasing the positive voltage U_{rev} sharpens the peak slightly. For all positive pulses we observe an increase in ion energy to a value some 10 eV below the energy equivalent of U_{rev}. In all cases, the IEDF's are broad in nature, rather than displaying a distinct peak energy as reported in Keraudy et al. [6] or Viloan et al. [14], a consequence of ion creation in the plasma with a potential that is slowly rising towards the set U_{rev} value over 10's of µs.

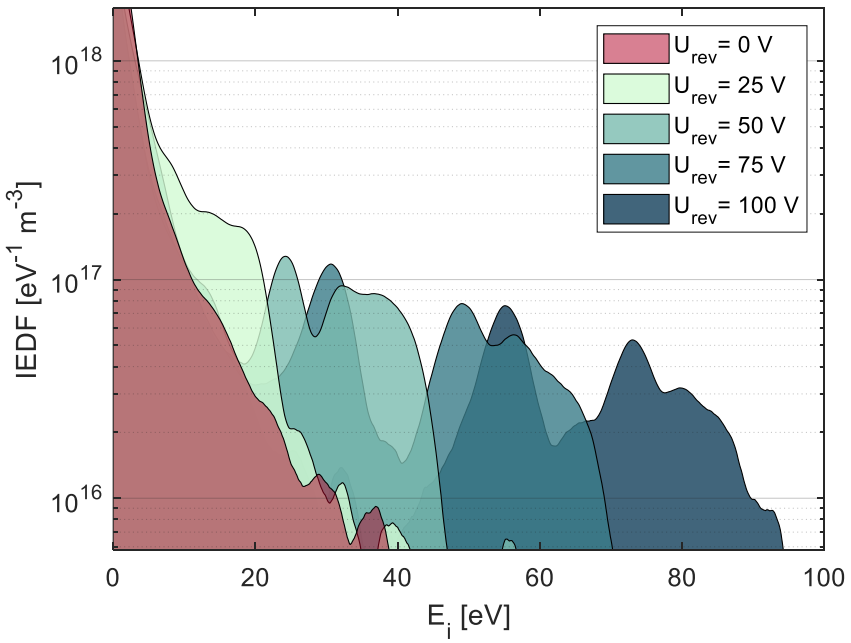

Figure 5. A plot of the time-averaged IEDFs for τ_{neg} = 70 µs for a variation in

positive pulses voltages from $U_{rev} = 0$ to 100 V.

In figure 6 a) and b) the time-evolution of the ion flux density Γ_i and energy flux density Q_i are shown for the different chosen U_{rev} values (from 0 to 100 V). These quantities are calculated using equations 3 and 4 respectively. We can see in figure 6a) that in the negative voltage pulse period U_{rev} has little effect on Γ_i however the ion fluxes are seen to decrease marginally in the positive pulse period as U_{rev} is increased. From the principle of conservation of ion flux (with no sinks or sources for ions), one should expect the flux of ions accelerated through different sheath voltages at the grounded entrance mesh, (G) in figure 1 to be independent of U_{rev}. The result may indicate therefore that either the plasma is denuded of ions in the bulk or the collection of ions by the RFEA is reduced by some geometric effect for higher values of U_{rev}.

Despite the slight decrease in Γ_i in the afterglow phase of the discharge due to the application of positive voltage pulses the energy flux density Q_i of ions falling to a grounded surface is dramatically increased. In fact, the energy flux of ions Q_i can greatly surpass that measured in the on-time of the HiPIMS pulse. We see in figure 6b) that Q_i peaks 10 μs into the reverse pulse at a value of 3×10^4 Wm^{-2}, some 6 times higher than the higher value in the negative voltage pulse. It is instructive to calculate the time-averaged values of ion flux density Γ_i and energy-flux density Q_i since the properties of a growing thin film will be influenced by these parameters over times much longer than the HiPIMS pulse period. These values are shown in table 1.

From the table we can see that the application of a positive pulse voltage of 100 V would (over the whole HiPIMS period) lead to a 16 % decrease in bombarding flux density however a five-fold increase in energy-flux density of ions bombarding a grounded thin film at the analyser location. Such a scenario, could enhance the ion-assisted film thin growth process leading to improved thin film densification as reported in Avino et al. [15].

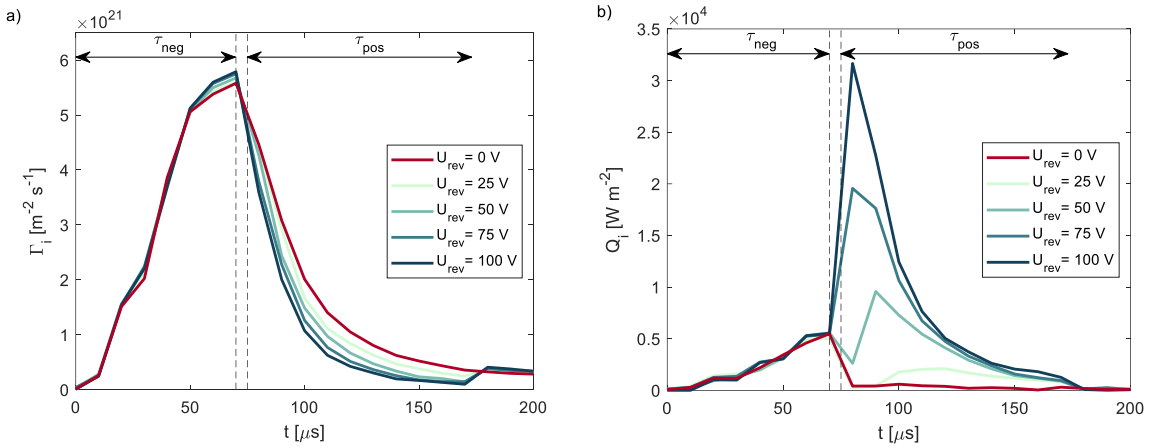

Figure 6. A plot of a) the ion flux density b) the energy flux density determined from measurements of the IEDF's for a variation in positive pulse voltages from U_{rev} = 0 to 100 V.

Table 1. The calculated time-averaged values of ion flux density Γ_i and energy-flux density Q_i for τ_{neg} = 70 μs and a range U_{rev} values. The discharge power was fixed at 200 W.

U_{rev} (V)	$\langle\Gamma_i\rangle$ $m^{-2}s^{-1}$	$\langle Q_i\rangle$ Wm^{-2}
0	1.95×10^{21}	1.08×10^{3}
25	1.86×10^{21}	1.63×10^{3}
50	1.77×10^{21}	3.02×10^{3}
75	1.70×10^{21}	4.41×10^{3}
100	1.64×10^{21}	5.31×10^{3}

3.2 The effect of τ_{neg} on $f_i(E)$, Γ_i and Q_i at a grounded electrode

The effect of changing the HiPIMS on-time τ_{neg} on the key ion bombarding metrics Γ_i and Q_i at a grounded electrode have been investigated for a constant discharge power of 200 W and positive pulse voltage U_{rev} = 50 V. The on-time duration is a key parameter in HiPIMS as it determines the size of the discharge current and hence the ultimate plasma density and the ion bombarding flux at the substrate. In addition, it governs the number of ions available in the afterglow that can continue ion bombardment during the plasma decay. It is an interesting feature of conventional HiPIMS that the decay times of the plasma (ion and electrons) are rather slow in afterglow [23].

Figures 7 (a- d) show the time-averaged IEDF's, as well as the time-evolution of discharge current I_d, ion flux density Γ_i and energy flux density Q_i for a range of τ_{neg} values from 40 to 130 µs. Please note the I_d, Γ_i and Q_i curves have been displayed with a shift in the time axis so that time t' = 0 represents the termination of the negative voltage pulse in each case. We see in figure 7a) a larger population of ions at high energy in the IEDF's for shorter τ_{neg} values. This may be due to increased discharge voltages as τ_{neg} is reduced, as shown in the lower part of figure 7b, leading to more high speed Nb atoms in the sputter velocity distribution, which are subsequently ionized in the plasma. Alternatively, reducing τ_{neg} may lead to higher fractions of sputtered metal ions in the IEDF's due to ion time-of-flight considerations as discussed by Viloan et al [14], where a short enough negative pulse is needed so that ions do not escape to the substrate before being accelerated by the positive pulse. The observed increased area under the $f_i(E)$ curves for small τ_{neg} values is consistent with higher measured discharge currents as seen in the upper part of figure 7b) with an 80 A increase in I_d over the τ_{neg} range.

The calculated ion flux densities Γ_i, shown in figure 7c), behave in a similar way to the discharge current in the negative pulse phase, as we may expect, with the bulk ion density scaling linearly (or at least following) I_d. In the positive pulse phase, however, there are significantly higher ion flux densities Γ_i measured as the τ_{neg} value is reduced. The decay rate in Γ_i also seems to

slow with smaller τ_{neg} values. Figure 7d) shows the calculated ion energy flux densities Q_i. Clearly as τ_{neg} is reduced, we observe higher and broader peaks in Q_i with peak value reaching 8 kWm^{-2} during the positive pulse. The time-average values for ion flux and energy-flux density are shown in table 2. We see that over the entire HiPIMS pulse period, decreasing the on-time τ_{neg} from 130 to 40 µs would result in a 25 % increase in the ion flux density and approaching a 4-fold increase in the ion energy flux density to a grounded substrate.

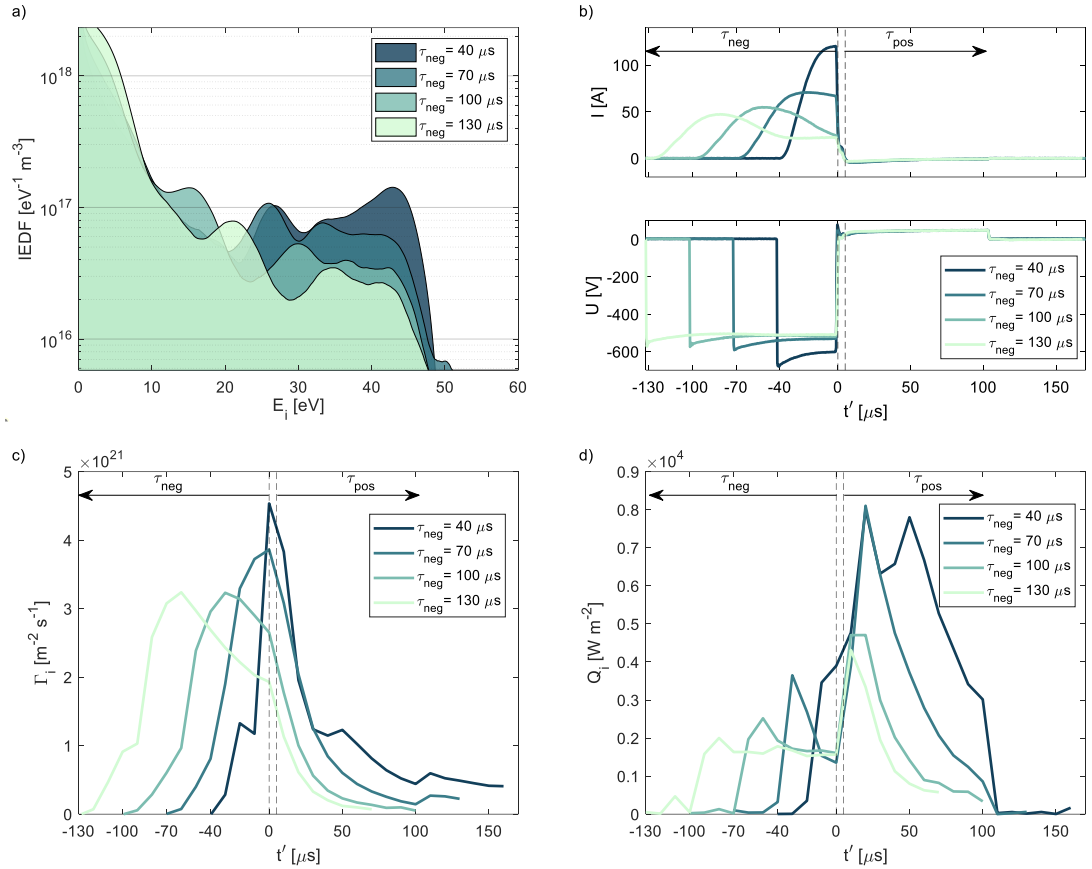

Figure 7. A plot of a) time-average IEDF's, as well as the time evolution of b) the discharge current I and voltage U, c) the ion flux density Γ_i and d) and the ion energy flux density Q_i for a variation of τ_{neg} from 40 µs to 130 µs. Please note, the time traces for I, Γ_i, and Q_i are shifted along the x -axis so that t' = 0 represents the termination of the negative voltage pulse phase (on-time) in each case.

Table 2. The calculated time-averaged values of ion flux density Γ_i and energy-

flux density Q_i for U_{rev} = 50 V and a range of τ_{neg} values.

τ_{neg} (µs)	$<\Gamma_i>$ $m^{-2}s^{-1}$	$<Q_i>$ Wm^{-2}
40	1.66×10^{21}	4.88×10^{3}
70	1.77×10^{21}	3.02×10^{3}
100	1.64×10^{21}	1.31×10^{3}
130	1.33×10^{21}	1.33×10^{3}

4. Discussion

The IEDF measurements show that the bipolar technique can increase the bombarding energy of ions (created in on-time plasma) to a grounded surface to values just short of the equivalent in the positive applied voltage eU_{rev}. After initiation of the reverse positive voltage, the plasma potential at the analyser position rises, over a period of 10's of µs, to reach a value just below the maximum applied U_{rev} setting. Time-resolved IEDF measurements show over this period ions in the plasma volume are accelerated through the rising plasma sheath [8] [10] established between the local plasma and grounded electrode at the analyser entrance. A double-layer structure responsible for ion acceleration as reported by Velicu et al [7], Tiron et al. [11], or Kozák et al. [12] was not believed to be present in this particular magnetron system geometry. Choosing higher U_{rev} values leads to a reduction in the measured ion flux density at the analyser. This may be due to a loss in collection efficiency of the analyser itself (an ion optic effect), or that plasma ions are redistributed in the bulk with enhanced loss to the grounded walls during this period. In other studies, the application of a reverse positive target bias has been seen to lead to a drop in the ion and electron density in the bulk plasma [24], possibly promoted by substantial ion accelerating sheaths at the vessel walls. This loss may be consistent with reports of decreased deposition rates observed in bipolar HiPIMS, operated in an unbalanced magnetron configuration, compared to the conventional unipolar technique [6] [10]. Whereas for a TriPack magnetic field configuration, which has an improved

deposition rate compared to the unbalanced configuration, a 19 % increase in deposition rate was observed by Wu et al. [25] using bipolar HiPIMS. Possible reasons why different magnetron systems show divergent behavior in the deposition rate when operating in bipolar HiPIMS mode are discussed briefly in [6] in terms of the degree of unbalance of the magnetron and the locality of the anode ring. Despite the fall in ion flux in this study, we have shown that the power density of ions accelerated to a ground substrate (and hence thin films) can be greatly increased with only the application of modest U_{rev} potentials, e.g. 100 V. Reducing the negative pulse length τ_{neg} at constant discharge power also has a major effect on the ion properties, namely by increasing on time-average the number of high energy ions bombarding a fixed bias surface with a correspondingly significant increase in the ion power density. It has been seen elsewhere that reducing the negative pulse lengths can reduce the presence of low energy bombarding metal ions [14].

5. Conclusions

A compact and robust retarding field energy analyser RFEA has been used for the first time to determine the ion energies during the different phases of an asymmetric bipolar HiPIMS discharge. A Langmuir probe has been used to calibrate the instrument for the incident positive ion flux and also determine the local plasma potential.

The effect of changing the negative voltage pulse duration τ_{neg} for the same applied power and the height of the positive voltage U_{rev} on the IEDF's was investigated. The results show that as the positive voltage pulse is applied, the local plasma potential V_p rises over 10's of μs up its maximum, just short of U_{rev}. The maximum measured ion energies are consistent with the sheath potential drop between the plasma (in which the ions were created) and the ground potential of RFEA entrance mesh. As τ_{neg} is shorted, larger ion flux densities can be seen in positive voltage pulse phase, coupled with a significant enhancement in the ion-energy flux density Q_i for ions bombarding at grounded substrate. We see a 4-fold increase in time-averaged Q_i when τ_{neg} is reduced from 130 to μs to 40 μs.

As the positive voltage U_{rev} is increased from 0 to 100V we observe a marginal reduction in the ion flux density in the positive voltage pulse phase, however a dramatic increase in the bombarding ion energy-flux density. On time-average, applying a U_{rev} of 100 V leads to a 5-fold increase in Q_i compared to the unipolar Urev = 0 V case.

The results from this RFEA study reveal the benefit of the bipolar HiPIMS technique in that, on time average the energy-flux density (power density) of ions bombarding a grounded (or fixed bias) thin film can be greatly increased as compared to the equivalent unipolar case. This has the potential to promote the ion-assisted deposition process and so enhance thin film quality.

Acknowledgements

We would like to thank the ASTeC Group, STFC Daresbury Laboratory, UK and the University of Liverpool for their funding support.

References

[1] M. Zanáška, D. Lundin, N. Brenning, H. Du, P. Dvorak, P. Vasina and U. Helmersson, "Dynamics of bipolar HiPIMS discharges by plasma potential probe measurements," *Plasma Sources Science and Technology,* vol. 31, January 2020.

[2] U. Helmersson, M. Lattemann, J. Bohlmark, A. P. Ehiasarian and J. T. Gudmundsson, "Ionized physical vapor deposition (IPVD): A review of technology and applications," *Thin Solid Films,* vol. 513, p. 1–24, August 2006.

[3] A. Anders, "A structure zone diagram including plasma-based deposition and ion etching," *Thin Solid Films,* vol. 518, p. 4087–4090, May 2010.

[4] G. Greczynski, I. Zhirkov, I. Petrov, J. E. Greene and J. Rosen, "Control of the metal/gas ion ratio incident at the substrate plane during high-power impulse magnetron sputtering of transition metals in Ar," *Thin Solid Films,* vol. 642, p. 36–40, November 2017.

[5] M. M. S. Villamayor, J. Keraudy, T. Shimizu, R. P. B. Viloan, R. Boyd, D. Lundin, J. E. Greene, I. Petrov and U. Helmersson, "Low temperature (Ts/Tm{\hspace{0.167em}}$\less${\hspace{0.167em}}0.1) epitaxial growth of {HfN}/{MgO}(001) via reactive {HiPIMS} with metal-ion synchronized substrate bias," *Journal of Vacuum Science & Technology A,* vol. 36, p. 061511, November 2018.

[6] J. Keraudy, R. P. B. Viloan, M. A. Raadu, N. Brenning, D. Lundin and U. Helmersson, "Bipolar HiPIMS for tailoring ion energies in thin film deposition," *Surface and Coatings Technology,* vol. 359, p. 433–437, February 2019.

[7] I.-L. Velicu, G.-T. Ianoş, C. Porosnicu, I. Mihăilă, I. Burducea, A. Velea, D. Cristea, D. Munteanu and V. Tiron, "Energy-enhanced deposition of copper thin films by bipolar high power impulse

magnetron sputtering," *Surface and Coatings Technology,* vol. 359, p. 97–107, February 2019.

[8] R. Hippler, M. Cada and Z. Hubicka, "Time-resolved diagnostics of a bipolar HiPIMS discharge," *Journal of Applied Physics,* vol. 127, p. 203303, May 2020.

[9] H. Du, M. Zanáška, N. Brenning and U. Helmersson, "Bipolar HiPIMS: The role of capacitive coupling in achieving ion bombardment during growth of dielectric thin films," *Surface and Coatings Technology,* vol. 416, p. 127152, June 2021.

[10] R. P. B. Viloan, U. Helmersson and D. Lundin, "Copper thin films deposited using different ion acceleration strategies in HiPIMS," *Surface and Coatings Technology,* vol. 422, p. 127487, September 2021.

[11] V. Tiron and I.-L. Velicu, "Understanding the ion acceleration mechanism in bipolar HiPIMS: the role of the double layer structure developed in the after-glow plasma," *Plasma Sources Science and Technology,* vol. 29, p. 015003, January 2020.

[12] T. Kozák, A. D. Pajdarová, M. Čada, Z. Hubička, P. Mareš and J. Čapek, "Ion energy distributions at substrate in bipolar HiPIMS: effect of positive pulse delay, length and amplitude," vol. 29, p. 065003, June 2020.

[13] A. D. Pajdarová, T. Kozák, Z. Hubička, M. Čada, P. Mareš and J. Čapek, "Plasma parameters in positive voltage pulses of bipolar HiPIMS discharge determined by Langmuir probe with a sub-microsecond time resolution," *Plasma Sources Science and Technology,* vol. 29, p. 085016, August 2020.

[14] R. P. B. Viloan, M. Zanáška, D. Lundin and U. Helmersson, "Pulse length selection for optimizing the accelerated ion flux fraction of a bipolar HiPIMS discharge," *Plasma Sources Science and Technology,* vol. 29, p. 125013, December 2020.

[15] F. Avino, D. Fonnesu, T. Koettig, M. Bonura, C. Senatore, A. T. P. Fontenla, A. Sublet and M. Taborelli, "Improved film density for coatings at grazing angle of incidence in high power impulse magnetron sputtering with positive pulse," *Thin Solid Films,* vol. 706, p. 138058, July 2020.

[16] M. Sode, T. Schwarz-Selinger and W. Jacob, "Quantitative determination of mass-resolved ion densities in H2-Ar inductively coupled radio frequency plasmas," *Journal of Applied Physics,* vol. 113, p. 093304, March 2013.

[17] I. S. Nedzelskiy, C. Silva, H. Figueiredo, H. Fernandes and C. A. F. Varandas, "Compact retarding field energy analyzer for the tokamak ISTTOK boundary plasma," *Review of Scientific Instruments,* vol. 77, p. 10E729, October 2006.

[18] D. Gahan, B. Dolinaj and M. B. Hopkins, "Retarding field analyzer for ion energy distribution measurements at a radio-frequency biased electrode," *Review of Scientific Instruments,* vol. 79, p. 033502, March 2008.

[19] S. Sharma, D. Gahan, P. Scullin, J. Doyle, J. Lennon, R. K. Vijayaraghavan, S. Daniels and M. B. Hopkins, "Measurement of deposition rate and ion energy distribution in a pulsed dc magnetron sputtering system using a retarding field analyzer with embedded quartz crystal microbalance," *Review of Scientific Instruments,* vol. 87, p. 043511, April 2016.

[20] S. G. Ingram and N. S. J. Braithwaite, "Ion and electron energy analysis at a surface in an RF discharge," *Journal of Physics D: Applied Physics,* vol. 21, p. 1496–1503, October 1988.

[21] P. Poolcharuansin, "The development of electrical plasma diagnostics for HiPIMS discharges," University of Liverpool, 2012.

[22] J. E. Allen, "On the plotting of electron and ion distribution functions," *Journal of Physics D: Applied Physics,* vol. 25, p. 1839–1840, December 1992.

[23] P. Poolcharuansin and J. W. Bradley, "Short- and long-term plasma phenomena in a HiPIMS discharge," *Plasma Sources Science and Technology,* vol. 19, p. 025010, February 2010.

[24] M. A. Law, F. L. Estrin, M. D. Bowden and J. W. Bradley, "Diagnosing asymmetric bipolar HiPIMS discharges using laser Thomson scattering," vol. 30, p. 105019, October 2021.

[25] B. Wu, I. Haehnlein, I. Shchelkanov, J. McLain, D. Patel, J. Uhlig, B. Jurczyk, Y. Leng and D. N. Ruzic, "Cu films prepared by bipolar pulsed high power impulse magnetron sputtering," *Vacuum,* vol. 150, p. 216–221, April 2018.